TU ELECTRIC

May 20, 1991

William J. Cahill, Jr.
Executive Vice President

U. S. Nuclear Regulatory Commission
Attn: Document Control Desk
Washington, D.C. 20555

SUBJECT: COMANCHE PEAK STEAM ELECTRIC STATION (CPSES)
DOCKET NOS. 50-445 AND 50-446
RESPONSE TO REQUEST FOR ADDITIONAL INFORMATION
REGARDING TOPICAL REPORT RXE-89-003,
"STEADY STATE REACTOR PHYSICS METHODOLOGY"

REF: Letter from James W. Clifford, NRC,
to William J. Cahill, Jr., TU Electric,
dated April 29, 1991

Gentlemen:

The NRC staff requested per the referenced letter, additional information to support the review of the subject topical report. Attachment 1 provides the TU Electric responses to the questions provided in the referenced letter.

In addition, copies of two summaries and one article are also provided for the convenience of the NRC reviewers.

1)   "Isotopic Depletion of Soluble Boron in a PWR," ANS Transactions, Vol. 57, p. 314. (Attachment 2)

2)   "Simulate-3 Pin Power Reconstruction Benchmarking Against B&W Critical Experiments," ANS Transactions, Vol. 56, p. 531. (Attachment 3)

3)   "CASMO-3: New Features, Benchmarking and Advanced Application," Nuclear Science and Engineering, Vol. 100, No. 3, p. 342. (Attachment 4)

If you should have questions regarding the attached responses, please call Jimmy Seawright at 214-812-4375 or Mickey Killgore at 214-812-8271.

Sincerely,

William J. Cahill, Jr.

By: D. R. Woodlan
D. R. Woodlan
Docket Licensing Manager

JDS/gj

c - Mr. R. D. Martin, Region IV
Resident Inspectors, CPSES (2)
Mr. J. W. Clifford, NRR

ADDITIONAL INFORMATION REGARDING
TOPICAL REPORT RXE-89-003,
"STEADY STATE REACTOR PHYSICS METHODOLOGY"

1. Question

Are all safety parameters to be calculated by TU Electric
(TUE) steady-state physics methodology included in Table 2.1
of the RXE-89-003-P report? If not, how will the
reliability factors for these essential parameters be
determined? Which code will be used to calculate each
safety parameter? Indicate the code to which the
reliability factors in Table 2.1 apply. Provide
benchmarking and reliability factors for all intended
code/parameter combinations which have not already been
included in RXE-89-003-P.

Response

The information provided in Table 2.1 specifically addresses
the small core criticals which were analyzed with
CASMO-3/PDQ-7.

The principal reactor physics parameters important to safety
analysis and calculated with the steady state models are
summarized in Table 6.1 with the exception of control rod
worth. The minimum uncertainty to be applied to each safety
parameter is shown in the total uncertainty column of Table
6.1. The control rod worth analysis is documented in
RXE-90-005 including the standard deviation between
calculated and measured control rod bank worths. For the
determination of control rod shutdown capability, a 10%
reduction in calculated rod worth is assumed, consistent
with the control rod worth acceptance criteria.

The SIMULATE-3 core model will be used to calculate steady-
state parameters, including control rod worth, for input to
the safety analysis.

The results shown in Table 6.1 were calculated with the
CASMO-3/SIMULATE-3 core model with the exception of the
local power uncertainty, which is based on results obtained
with CASMO-3/PDQ-7.

As discussed in Section 4.6 of RXE-89-003-P, the SIMULATE-3 core model will be utilized to obtain best estimate power peaking using pin power reconstruction. The SIMULATE-3 pin power reconstruction methodology combines nodal diffusion theory with pin-by-pin transport theory. SIMULATE-3 overlays assembly pin-by-pin power distributions, determined with CASMO-3, onto the nodal diffusion theory results. This methodology for determining power peaking has been verified by TU Electric and approved by the NRC for use by Yankee Atomic (SIMULATE-3 Validation and Verification, YAEC-1659-A, September, 1988). The application of the local power uncertainty to SIMULATE-3 is conservative since the combined transport theory-diffusion theory results are more accurate than pin-by-pin diffusion theory results. The capability of the SIMULATE-3 pin power reconstruction method to accurately predict pin power distribution for critical experiments is summarized in "SIMULATE Pin Power Reconstruction Benchmarking Against the B&W Critical Experiments," ANS Transactions, Vol. 56, p 531.

2. Question

Discuss the applicability and completeness of the Catawba-1 and Prairie Island-1 benchmarking for the intended Comanche Peak Steam Electric System (CPSES) reload fuel designs and operating conditions. What new fuel designs will be used in CPSES and how will differences relative to the benchmarking data base be accounted for?

Response

Catawba Unit 1, Cycles 1 and 2 were selected for benchmarking because of the following similarities to Comanche Peak Steam Electric Station (CPSES):

4 Loop Westinghouse Plant, 3411 MWt

Low enrichment first core (1.60 w/o, 2.4 w/o, 3.1 w/o)

Pyrex burnable absorber design, the same as CPSES Unit 1, Cycle 1

Optimized fuel assembly design, the same as CPSES Unit 2, Cycle 1

Hot full power average moderator temperature of 592.5° F, as compared to the CPSES temperature of 591.5° F

Prairie Island Unit 1, Cycles 6 through 10 were chosen for benchmarking because of the reload fuel design features which are similar to those planned for CPSES. Those design features include:

> Co-resident Westinghouse and Advanced Nuclear Fuel, (ANF) reloads
>
> Natural uranium axial blankets
>
> Employment of gadolinia as a burnable absorber
>
> Mixed core including fuel assembly designs of various water-to-fuel ratios

In addition, differences among the three plants permit the models to be challenged over a range of parameters.

> Prairie Island is a two loop Westinghouse plant, 1650 MWt with a 14 x 14 fuel assembly lattice
>
> Prairie Island has a hot full power average moderator temperature of 560°F
>
> Catawba Unit 1 employs B_4C control rods while Prairie Island employs Ag-In-Cd control rods

The CPSES Unit 1, Cycle 1 core and Cycle 2 reload utilize fuel of standard Westinghouse design. The Cycle 1 core employs pyrex burnable absorbers while the Cycle 2 reload employs Wet Annular Burnable Absorber (WABA) rods. TU Electric analyses of CPSES Unit 1, Cycles 1 and 2 are performed in parallel with Westinghouse, providing a comprehensive overcheck. In addition, the measured results obtained to date have verified the TU Electric calculations.

The CPSES, Unit 2, Cycle 1 core will utilize Westinghouse Optimized Fuel Assemblies (OFA) and WABA rods. The OFA design has been addressed with the Catawba benchmarking. The analyses of CPSES, Unit 2, Cycle 1 will also be performed in parallel with Westinghouse.

The ANF reloads, Cycle 3 and beyond for Units 1 and 2, are expected to include standard fuel, natural uranium axial blankets, and gadolinia as a burnable absorber. The mechanical design features of the ANF fuel differ little from the current Unit 1 fuel in the region of the active core. Natural uranium axial blankets and gadolinia, up to 4 w/o, have been included in the Prairie Island comparisons.

The preliminary design for Unit 1, Cycle 3, is an annual
cycle employing 5 w/o gadolinia. Subsequent cycles for Unit
1, and Cycles 2 and beyond for Unit 2, have not been
designed. However, in the long term, the CPSES Units may
operate on extended cycles. Under the existing contracts,
the most economically attractive burnable absorber for an
extended cycle is gadolinia. It is anticipated that
concentrations in the range of 8 w/o to 10 w/o would be
required. Employment of gadolinia concentrations in this
range will require additional work to quantify the
reliability of the TU Electric methodology. The most
appropriate route for extending the methodology has not been
decided. Approaches to be considered include demonstration
programs, benchmarking with measured data from other power
reactors, or benchmarking with fuel vendor analyses.

3.   Question

How was the axial buckling for the pin cell critical
experiments determined? How is the (+0.00074) k_{eff} accuracy
and the (+0.0047) bias used in TUE methodology? How was the
radial leakage accounted for in the CASMO-3 pin-cell
calculations?

Response

The buckling values (axial and radial leakage) used for the
pin cell critical calculations described in Table 5.1 are
those determined during the measurements and reported in
Reference 18 of RXE-89-003-P.

The k_{eff} accuracy and bias given in Tables 5.9 and 5.10 apply
to small core criticals and are not used explicitly in the
TU Electric methodology. The bias is unique to the small,
high leakage cores and is not propagated to large cores.
These calculations were performed to demonstrate the
applicability of the large power reactor methodology by
comparison to well defined benchmark experiments. This
methodology includes use of the standard 40-group CASMO-3
library for cross section data and employment of seven
energy groups for the transport solution. The PDQ-7 core
model uses two-group conventional cross sections with G-
factors applied to water holes and burnable absorber rods,
and a mesh interval spacing equal to one pin pitch was used
within the cores. The results of the comparisons, when
corrected for identified modeling approximations, provide
additional verification of the accuracy of CASMO-3 in a
"production mode."

4. Question

    Discuss the applicability of the small-core criticals and
    associated local power peaking reliability factors to the
    intended CPSES fuel designs. Do the comparisons used to
    determine the local power peaking reliability factors
    indicate larger differences for the high powered rods and,
    if so, how is this accounted for? What was the basis for
    excluding "suspect" data from the small core critical
    comparisons, and what is the effect of including this data
    on the local power peaking reliability factor?

    Response

    The small core criticals are applicable to CPSES fuel
    designs and were selected to encompass important
    characteristics of planned CPSES reloads. These
    characteristics include water holes, gadolinia-bearing fuel,
    pyrex burnable absorber rods, and lattice configurations
    typical of a PWR.

    Comparisons used to determine local power peaking
    reliability factors do not indicate larger differences if
    only high power rods (relative power >1.0) are used. Using
    only high power rods reduces the calculational
    uncertainties. Table 1 lists the total standard deviations
    for all pins excluding suspect data and the corresponding
    values calculated with only the high power pins.

    Suspect pin data was excluded from two small core
    comparisons based on the following evaluation. The measured
    power in each pin was compared to that in surrounding pins.
    If the value appeared noticeably inconsistent with its
    neighbors, a comparison was made between a transport theory
    corrected calculated value and the measured value. If
    transport theory results confirmed a discrepancy in the
    measured result, that pin was excluded from the data set.
    Only two pins were excluded.

    Figure 1 shows the results for Core XI Loading 2 with the
    suspect data retained. Figure 2 shows the transport
    corrected result.   The measured results for the pin in core
    location row 8, column 4 is obviously suspect.

    Figure 2 also illustrates the improvement in calculated-to-
    measured comparisons which are obtained with transport
    theory.

Table 2 illustrates the effect on the local power
uncertainty of including the suspect pins. Core XI Loadings
2 and 3 contain the suspect pins. Dropping the suspect data
reduces the overall calculational standard deviation from
1.777 to 1.731.

Table 1
Small Core Criticals - Standard Deviation in Calculated +
Measured Relative Power Distributions
Use of All Pins Versus Use of Only High Power
(Relative Power > 1.0) Pins

Core	Loading No.	All Pins	Only High Power Pins
XI	2	1.8451	2.1857
	3	1.6833	1.9913
	4	2.3176	2.1090
	5	2.1833	1.8964
	6	2.0949	1.7284
	7	1.7636	1.4063
	8	2.2372	1.6702
	9	1.9432	1.4126
	11	1.5287	1.6468
XII	1	2.1875	2.1985
Gd	1	1.5936	2.1688
	5	1.7240	1.6667
	12	1.6974	2.1322
	14	2.3526	1.8367
Overall Measured+ Calculated Standard Deviation		1.959	1.880

Table 2
Small Core Criticals - Standard Deviation in Measured and
Calculated Relative Power Distributions - Suspect Data Included

Core	Loading No.	Standard Deviation of Meas.+Calc.	Standard Deviation of Meas. Data	Standard Deviation of Calc. Data
XI	2	2.1312	1.2934	1.6939
	3	1.9800	0.9121	1.7574
	4	2.3176	0.7630	2.1884
	5	2.1833	0.8811	1.9976
	6	2.094ª	0.6083	2.0046
	7	1.7636	0.9819	1.4650
	8	2.2372	1.0886	1.9545
	9	1.9432*	0.9083	1.7179
	11	1.5287	1.2652	0.8581
XII	1	2.1875	1.3096	1.7522
GD	1	1.5936	0.3096	1.5632
	5	1.7240	0.7657	1.5447
	12	1.6974	0.4897	1.6252
	14	2.3526	0.5438	2.2889
Overall Calculational Uncertainty =				1.777

* Reported in RXE-89-003-P as 1.9568 with one pin inadvertently excluded.
Inclusion of the pin in the analysis has no effect on overall
calculational standard deviation of 1.731.

FIGURE 1. SMALL CORE CRITICALS CORE XI LOADING 2
MEASURED VS CASMO-3/PDQ-7 RELATIVE POWER
DISTRIBUTION - ALL DATA USED

	1	2	3	4	5	6	7	8
1	H2O							
2	FUEL -1.0 1.074 1.063	FUEL +2.1 1.036 1.058	%DIF Measured CASMO-3/PDQ-7					
3	FUEL +2.3 0.996 1.019	FUEL +1.1 1.043 1.055	H2O					
4	FUEL +3.0 0.970 1.000	FUEL +2.5 1.005 1.03u	FUEL -1.7 1.083 1.065	FUEL +1.3 1.059 1.072				
5	FUEL -0.2 0.995 0.993	FUEL +0.8 1.016 1.024	FUEL -2.0 1.085 1.063	FUEL -2.4 1.111 1.084	H2O			
6	FUEL -0.7 0.996 0.989	FUEL -3.1 1.065 1.032	H2O	FUEL -3.0 1.099 1.066	FUEL -3.8 1.076 1.035	FUEL +0.7 0.985 0.992		
7	FUEL +2.1 0.951 0.971	FUEL -0.1 0.996 0.995	FUEL -1.9 1.038 1.019	FUEL -0.1 1.001 1.000	FUEL -0.7 0.977 0.970	FUEL +0.6 0.944 0.950	FUEL -0.9 0.941 0.933	
8	FUEL -0.4 0.954 0.950	FUEL -1.8 0.973 0.956	FUEL +2.9 0.932 0.960	FUEL +6.4 0.897 0.954	FUEL -0.3 0.945 0.942	FUEL -1.2 0.942 0.931	FUEL -0.1 0.922 0.921	FUEL +2.0 0.893 0.911

MAXIMUM POWER   Measured   .... 1.111 ROW 5 COLUMN 4
                CASMO-3/PDQ-7....... 1.084 ROW 5 COLUMN 4
% DIFFERENCE: MAXIMUM........... +6.390 ROW 8 COLUMN 4
                AVERAGE ABSOLUTE.. +1.670

FIGURE 2. SMALL CORE CRITICALS CORE XI LOADING 2 MEASURED VS
TRANSPORT THEORY CORRECTED RELATIVE POWER DISTRIBUTION

	1	2	3	4	5	6	7	8
1	H2O							
2	FUEL −0.4 1.074 1.070	FUEL +0.4 1.036 1.041	%DIF Measured TRANSPORT THEORY CORRECTED					
3	FUEL +1.3 0.996 1.008	FUEL +2.4 1.043 1.068	H2O					
4	FUEL +2.2 0.970 0.991	FUEL +1.1 1.005 1.016	FUEL −0.3 1.083 1.080	FUEL −0.3 1.059 1.056				
5	FUEL −0.9 0.995 0.985	FUEL −0.4 1.016 1.012	FUEL −0.5 1.085 1.079	FUEL −1.2 1.111 1.097	H2O			
6	FUEL −1.3 0.996 0.983	FUEL −1.5 1.065 1.050	H2O	FUEL −1.7 1.099 1.080	FUEL −2.1 1.076 1.053	FUEL −0.1 0.985 0.984		
7	FUEL +1.6 0.951 0.966	FUEL −0.9 0.996 0.987	FUEL +0.0 1.038 1.039	FUEL −0.9 1.001 0.992	FUEL −1.1 0.977 0.966	FUEL +0.4 0.944 0.948	FUEL −0.9 0.941 0.933	
8	FUEL −0.6 0.954 0.949	FUEL −2.2 0.973 0.952	FUEL +2.5 0.932 0.956	FUEL +6.0 0.897 0.950	FUEL −0.4 0.945 0.941	FUEL −1.2 0.942 0.931	FUEL −0.1 0.922 0.921	FUEL 2.2 0.893 0.913

```
MAXIMUM POWER   Measured      .......  1.111 ROW 5 COLUMN 4
                calculated..........  1.097 ROW 5 COLUMN 4
% DIFFERENCE:   MAXIMUM...........  +5.975 ROW 8 COLUMN 4
                AVERAGE ABSOLUTE..  +1.217.
```

5.   Question

Were the procedures and code options used in the
benchmarking analyses the same as will be used in the CPSES
licensing analyses? If not, discuss the differences and
expected impact on the reliability factors.

Response

The procedures and code options used in the benchmarking
analyses were selected to be the same as will be used in the
CPSES licensing analysis. However, detail modeling
improvements are anticipated as additional CPSES operating
data becomes available. These modeling improvements are
expected to reduce the differences between calculated and
measured results and consequently confirm the conservatism
in the reported uncertainties.

6.   Question

Provide the details of the isothermal temperature
coefficient (ITC) measurements discussed in Chapter 5. What
fraction of the measured ITCs is due to the Doppler
coefficient? Since these measurements are being used to
infer the moderator coefficient calculational uncertainty,
discuss the applicability of these beginning-of-life, hot-
zero-power results to typical operating conditions.

Response

The isothermal coefficients presented in Chapter 5 were
determined as a part of the startup physics testing for the
respective cores and cycles. The measurements were made by
alternately cooling and heating the primary system. The
change in primary coolant temperature was measured with
standard plant instrumentation and the change in reactivity
was inferred with the reactivity computer.

Specific values of the Doppler temperature coefficient at
hot zero power have been calculated for Prairie Island Unit
1, Cycle 7 and CPSES Unit 1, Cycle 1. The results are -1.8
pcm/$^{\circ}$F and -1.9 pcm/$^{\circ}$F, respectively, indicating only a
small sensitivity to the core designs. Adding the CPSES
Unit 1, Cycle 1 startup test results to the isothermal
coefficient data presented in Table 6.6 of RXE-89-003-P, the
inferred moderator temperature coefficients are shown below.

| Plant | Cycle | pcm/°F | | |
		Iso.	Dop.	Mod.
PI1	6	-3.6	-1.8	-1.8
	7	-1.9	-1.8	-0.1
	8	-3.6	-1.8	-1.8
	9	+1.3	-1.8	+3.1
	10	-3.1	-1.8	-1.3
Catawba 1	1	-1.7	-1.9	+0.2
	2	+1.7	-1.9	+3.6
CPSES 1	1	-1.0	-1.9	+0.9

The moderator temperature coefficient varies smoothly with
temperature and boron concentration, and responds modestly
to core exposure. The Doppler coefficient varies smoothly
with fuel temperature and core exposure (plutonium buildup).

Measurements at beginning of life, hot-zero power serve to
confirm the integrated ability of the model (including the
effects of isotopics, boron concentration, cross sections
and flux importance weighting) to predict the coefficient.
Because of the smoothly varying functionality of the
moderator coefficient and the fidelity of the basic
microscopic cross section data, the uncertainty based on
beginning-of-cycle, hot-zero power comparisons can be
extended over the range of typical operating conditions.

7. Question

    In order to reduce the calculation reliability factors for
    the boron endpoint, boron letdown, isothermal temperature
    coefficient and local pin powers, the measurement error has
    been subtracted from the observed calculation-to-measurement
    standard deviation. The calculation of the 95/95
    reliability factor in this case required the 95 percent
    confidence limit on the measurement error, which is
    determined by the number of samples used to determine the
    measurement error. If the measurement error is to be
    subtracted, provide the statistical basis for the
    measurement error, including the number of samples used in
    the determination.

    Response

    The measurement error used in the local pin power
    uncertainty calculations comes from the data reported in
    References 20 through 22 of RXE-89-003-P. The difference

distributions for the relative pin powers include both
calculational and measurement uncertainty. An overall
variance was computed using the square root of the sum of
the squares of the differences. The measurement variance is
computed as the sum of squares of the measured standard
deviations. Each measured pin has a specific measurement
error provided. These measurement errors are always less
than the calculational uncertainty. The calculational
variance is then the difference between the variance of the
difference distribution and the measurement variance. The
95/95 one-sided upper tolerance limit factor is applied
after the difference is computed.

The errors associated with the boron end point and the boron
letdown measurements are not readily available. The
difference distributions used in the uncertainty
calculations contain both measured and calculational error.
The estimate of the measurement error for the boron end
point was chosen to account for the minimum measurement
error which might be expected. The error applied in the
boron letdown analysis is the error associated with using a
single line to represent scattered data and is discussed
further in the response to question 8. The impact of these
choices can be seen by assuming no measurement error:

		With Meas. Error	Without Meas. Error
Boron End Point		-75.6 ppm	-82.2 ppm
Boron Letdown	0-1500 MWD/MT	-63.0 ppm	-67.7 ppm
	>1500 MWD/MT	-37.8 ppm	-42.6 ppm
	EOC	-17.5 ppm	-27.8 ppm

The reliability factor data assuming no measurement error
are obtained from Tables 6.2 through 6.5 using the rms
standard deviation rather than the standard deviation of the
calculated values. The boron letdown reliability factor has
been evaluated for design purposes but is not required for
the safety analysis.

The isothermal temperature coefficient reliability factor
presented in Table 6.6 of RXE-89-003-P has been recalculated
assuming no measurement error. Consistent with the control
rod worth analysis presented in RXE-90-005, data for Prairie
Island Unit 1, Cycle 8 have been excluded and data for
Comanche Peak Unit 1, Cycle 1 have been added. The results
are given in Table 3.

Table 3
Reliability Factor Analysis - Isothermal Temperature Coefficient

Plant	Cycle	pcm/oF Calculated	Measured	pcm/oF Difference
PI 1	6	-2.45	-3.60	1.15
	7	-1.85	-1.90	0.05
	9	2.45	1.30	1.15
	10	-2.25	-3.10	0.85
CATAWBA	1	-2.75	-1.70	-1.05
	2	1.85	1.70	0.15
CPSES 1	1	-0.70	-1.00	0.30
average				+0.371
rms standard deviation				+0.776
standard deviation of Measured				+0.000
standard deviation of Calculated				+0.776
Reliability factor				+2.639
Bias				+0.371
Total uncertainty				+3.010

8. Question

    Why has the boron measurement error been removed from the
    observed calculation-to-measurement standard deviation for
    the boron letdown comparisons, when in fact the measured
    boron data has been "smoothed" to eliminate the measurement
    error.

    Response

    The smoothing of the data certainly reduces the measurement
    error. This is apparent by an examination of the
    differences before and after the smoothing process.
    However, what remains is the error in drawing the line; that
    is, how well the line represents the measurement. If only
    one line were possible, the error would be zero. However,
    the least squares piecewise fits provide the "best" line in
    the least squares sense. The curve fitting error obtained
    from the least squares analysis used for the boron letdown
    then provides a measure of how well the line is drawn and is
    therefore included in the analysis.

    It should also be noted that the boron letdown uncertainty
    is used to gain insight into modeling accuracy. This
    uncertainty is not used in any safety analyses.

9. Question

    Determining the Doppler temperature coefficient (DTC)
    reliability factor by comparing TUE predictions with other
    calculations does not include the as-built and operational
    DTC error components and, therefore, does not provide a true
    estimate of the DTC calculational uncertainty. Provide
    additional justification for the DTC reliability factor.

    Response

    Comparisons of Doppler temperature coefficients calculated
    with CASMO-3 to measurements performed by Hellstrand are
    presented in a technical paper, "CASMO-3: New Features,
    Benchmarking, and Advanced Application," Nuclear Science and
    Engineering, Vol. 100, No. 3, P. 342, November, 1988. These
    measurements were for UO_2 fuel rods with various radii and
    encompassed a temperature range of 80°F to 1400°F. Table 4
    shows the results of the uncertainty analysis. The
    reliability factor of 9 percent further substantiates the
    conservatism in the fuel temperature coefficient uncertainty
    of 10 percent specified in Table 6.1 of RXE-89-003-P.

Table 4

Reliability Factor Analysis - Doppler Coefficient
CASMO-3 Comparison with Measurement

Cases from Reference 1	b/ $\sqrt{Fuel\ Temp}$		%Difference
	CASMO-3	Measured	
CASE-1	8.249E-03	8.2E-03	5.976E-01
CASE-2	7.866E-03	7.6E-03	3.500E+00
CASE-3	6.853E-03	7.0E-03	-2.100E+00
CASE-4	6.687E-03	6.7E-03	-1.940E-01
CASE-5	6.342E-03	6.4E-03	-9.062E-01
average			+0.179
rms standard deviation			+2.104
standard deviation of Measured			+0.000
standard deviation of Calculated			+2.104
Reliability factor			+8.85
Bias			+0.18
Total uncertainty			+9.02

10. Question

Why is the W calculated end-of-cycle critical boron concentration outside the 95/95 tolerance limit for both the TUE PDQ-7 and SIMULATE-3 calculations?

Response

The most recent estimate provided by W for the end-of-cycle 1 exposure is 12,600 ± 300 MWD/MT, corresponding to a boron concentration of 10 ppm. W included the as-built assembly masses and enrichments in that estimate. The TU Electric analysis presented in RXE-89-003-P, based on nominal design enrichments and masses, results in a projected end-of-cycle of 12,100 ± 300 MWD/MT (the TU Electric EOC uncertainty of 21 ppm corresponds to an exposure uncertainty of 300 MWD/MT). Sensitivity studies performed by TU Electric show that including as-built fuel data increases the critical boron concentration near end-of-cycle by at least 10 ppm. Including this effect in the analysis would result in a projected cycle length of 12,250 ± 300 MWD/MT with SIMULATE-3 and slightly longer with PDQ-7. With the projected cycle lengths adjusted to the same bases, there is nearly full overlap on the uncertainties between the Westinghouse calculations and the TU Electric calculations.

11. Question

Both PDQ-7 and SIMULATE-3 analyses of the Catawba-1 boron letdown curves show an underprediction of the boron concentration throughout most of Cycle 1. SIMULATE-3 also underpredicts the letdown curves for Prairie Island Cycles 5-10. Is this underprediction expected in the Comanche Peak-1 calculations? What is the measured vs. calculation experience thus far in Cycle 1?

Response

The differences between the calculated and measured boron letdown curves were extensively reviewed for both Catawba Unit 1 and Prairie Island Unit 1. The following observations have been made:

a. The cycle exposure corresponding to a Hot Full Power critical boron concentration of 10 ppm can be consistently predicted with SIMULATE-3.

b. Fuel cycles which contain mostly fresh fuel at the start
    of the cycle, typically Cycle 1, will show an
    underprediction of boron during most of the cycle when
    using CASMO-3/SIMULATE-3 or CASMO-3/PDQ-7.

c. The underprediction in boron concentration is much less
    pronounced in reload cycles.

d. The apparent underprediction in Prairie Island is
    amplified by the burnout of B-10 in the soluble boron.
    This phenomenon has been confirmed for several PWRs
    including subsequent cycles in Prairie Island. The
    magnitude of the effect is projected to be between 20
    ppm and 40 ppm.

Based on the above, an underprediction was expected for
CPSES Unit 1, Cycle 1. The calculated and measured boron
letdown curve for CPSES Unit 1, Cycle 1 is presented in
Figure 3.

12. Question

Collapsing the full core measured power distribution to an
eighth-core or quarter-core representation reduces the
calculations-to-measurement differences and inferred
calculational uncertainty. What is the increase in the
calculational uncertainty when a full-core representation is
used?

Response

The full core measurements reflect any core design
asymmetrics as well as the effects of as-built properties,
measurement uncertainties, temperature variations, and
variations in burnup propagated from cycle to cycle. The
collapse to eighth-core or quarter-core was employed to
provide the most consistent comparison with the analytical
model.

The calculational uncertainties associated with a full-core
calculated to measured power distribution comparison are
similar to the differences between the full-core calculated

FIGURE 3.   COMANCHE PEAK STEAM ELECTRIC STATION UNIT 1,
            CYCLE 1, BORON LETDOWN
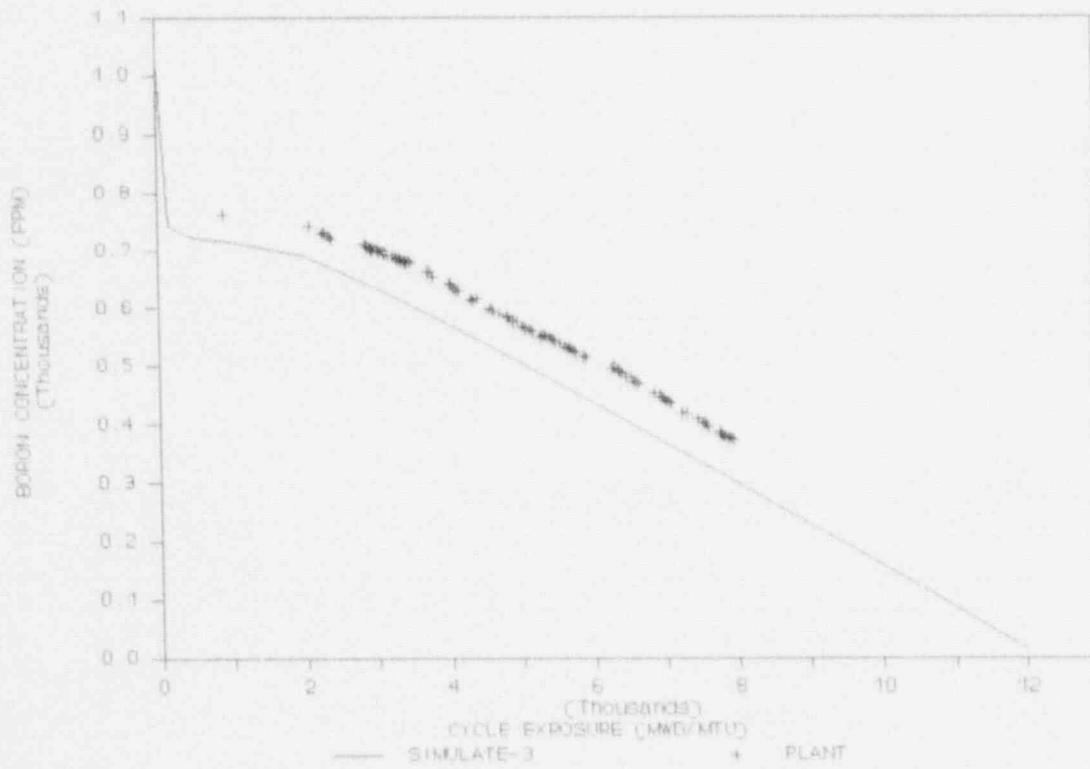
and measured relative reaction rates. The differences
between calculated and measured assembly relative powers are
inferred from the differences between calculated and
measured relative reaction rates.

The following comparisons are made for Catawba Unit 1, Cycle
1, using data presented in RXE-89-003-P. Similar
comparisons can be made for Catawba Unit 1, Cycle 2.

	Full-Core Measured	Quarter-Core PDQ-7	Eighth-Core Simulate-3
Fig.	5.8	5.15	5.24
Ave.	5.2%	2.9%	4.2
Max.	+15.0%	-6.4%	-8.7%
Fig.	5.9	5.16	5.25
Ave.	1.4%	0.6%	1.7%
Max.	+7.0%	+2.1%	+4.9%
Fig.	5.10	5.17	5.26
Ave.	1.3%	0.9%	1.2%
Max.	+6.8%	-2.9%	+3.6%
Fig.	5.11	5.18	5.27
Ave.	1.6%	1.0%	1.4%
Max.	+7.1%	-2.1%	+2.9%

The relative power distribution comparisons are presented to
illustrate model acceptability. No reliability factors have
been computed for application in the safety analysis.

13. Question

How do radial and axial reflector parameters differ in the
Catawba-1, Prairie Island-1, and Comanche Peak-1
calculations? How will reflector parameters vary from cycle
to cycle?

Response

The radial and axial reflector cross sections are calculated
with CASMO-3 using the reflector option. The reflector
option allows the thickness and composition of the reflector
regions to be specified based on the actual reactor
dimensions and characteristics. Cross sections for the fuel
region are generated using the same micro and macro group
calculations performed in assembly calculations. The fuel
is used to obtain a flux spectrum in the reflector region.

Explicit axial and radial reflector descriptions were used
in the CASMO-3 models to generate reflector cross sections
for Catawba-1, Prairie Island-1 and Comanche Peak Unit 1.
SIMULATE-3 requires the reflector cross sections and
discontinuity factors to be modelled as a node external to
the active fuel region. For the PDQ-7 model, the baffle
cross sections are edited for a two-pin pitch width
containing a small amount of reflector water homogenized
with the steel baffle. The PDQ-7 model includes a water
reflector region adjacent to the baffle.

In the radial reflector, the one dimensional multi-region
transport model includes a fuel region, a stainless steel
baffle and a water reflector region. For Prairie Island
Unit 1, the baffle is 1.125 inches thick and for Catawba
Unit 1 and Comanche Peak Unit 1 the baffle thickness is
0.875 inches. All three radial reflector transport models
used a 6 inch water region adjacent to the baffle.

For the top and bottom reflectors, a model similar to the
radial reflector model is employed. The one dimensional
axial model was developed by radially homogenizing the
zircaloy core components, stainless steel structure, and
water above and below the fuel region, respectively. For
each reactor, the axial reflector regions were modelled
consistent with the design of the core components as well as
the fuel parameters.

Sensitivity studies have been performed to investigate the
effect of various reactor parameters on the reflector cross
sections and the SIMULATE-3 results. Reflector cross
sections were calculated for various fuel and moderator
temperatures, fresh and burned fuel, and different fuel
enrichments. These studies indicate only a small
sensitivity in power shape and core reactivity for the range
of parameters considered.

There are no adjustable parameters such as albedos or
thermal leakage correction factors used in the models. The
reflector cross sections for Comanche Peak are not
anticipated to vary from cycle to cycle.

generated by the ADC (Ref. 2). The correlation coefficient was 0.9997.

The computed reactivity was displayed on a homemade readout panel. An IBM-supplied subroutine in LOGGER was used to output the individual digits of the reactivity value (algebraic sign, leading digit, decimal point, and three fractional digits).

RESULTS

Figure 1 illustrates the measured reactor power and calculated reactivity for a 70¢ step change in reactivity. These data were taken at 1-s time intervals. It is seen that the reactivity, initially at zero, rises rapidly to a predetermined value (determined by the reactivity change induced in the system) and then returns to zero as the reactor is reestablished in a critical situation by insertion of another control rod.

SUMMARY

The method of Tuttle[1] has been adapted to produce a reliable, on-line calculation of reactivity from a time-dependent reactor power signal. Rapid reactivity changes can be measured. Reactivity changes associated with reactor pulses will be discussed in a subsequent paper.

1. R. J. TUTTLE, "Elimination of the Effect of a Constant Neutron Source in Reactivity Measurement," NAA-SR-MEMO-12290REV, Atomics International, Canoga Park, California (1967).

2. ALLA J. M. BAKIR, "Development of a Personal Computer-Based Reactivity Meter for a Research Reactor," MS Thesis, Oregon State University (1988).

ANS TRANSACTIONS   Vol 57

9. Isotopic Depletion of Soluble Boron in a PWR,

José M. Aragonés (DENIM-Spain), Carol Ahnert (CIEMAT-Spain), Antonio Crespo (DENIM-Spain), José R. León (C. N. Almaraz-Spain)

The purpose of the work reported in this paper is to determine the isotopic depletion of the soluble boron in the primary of a pressurized water reactor (PWR) along cycle operation under the limiting condition of continuous boron dilution without fresh boron feeding, which maximizes the boron isotopic depletion effect. Presented here are the results for cycle 4 of the C. N. Almaraz-II PWR, which has been operated close to these continuous dilution conditions at rated power throughout most of the cycle.

In the continuous boron dilution model, the boron concentration letdown curve $B(t)$, i.e., in parts per million of total boron weight along time, is achieved by adjusting the mass flow feed of clean water $G_f(t)$, equal to the mass flow bleed of borated water from the primary with a constant total water mass inventory M_p. The balance equation for the total boron mass in the primary is given by

$$\frac{d}{dt} B(t)M_p = -B(t)G_f(t) . \tag{1}$$

Hence, the integrated feed mass of clean water required to reduce the boron concentration from $B(0)$ to $B(t)$ is given by

$$M_f(t) = \int_0^t G_f(t) \, dt = M_p \ln \frac{B(0)}{B(t)} , \tag{2}$$

To determine the isotopic abundance in ^{10}B of the soluble boron in the primary, $e(t)$ in weight, the balance equation for the total ^{10}B mass in the primary should include the neutron absorptions integrated in the whole core and surrounding irradiation volumes, as given by

$$\frac{d}{dt} e(t)B(t)M_p = -e(t)B(t)G_f(t) - e(t)B(t)M_c \langle \sigma_a^{10B}\Phi \rangle , \tag{3}$$

obtaining

$$e(t) = e(0) \exp\left[-\frac{M_c}{M_p} \int_0^t \langle \sigma_a^{10B}\Phi \rangle \, dt \right] , \tag{4}$$

where M_c is the total mass of water in the active core volume and $\langle \sigma_a^{10B}\Phi \rangle$ is the average ^{10}B absorption probability in the active core per unit time. The ratio of core to primary water mass, M_c/M_p, ~6% in the C. N. Almaraz PWR, is essential to avoid a very quick ^{10}B depletion in the soluble boron, since the absorption probability is higher than in lumped burnable absorbers with spatial self-shielding by flux depression.

The calculation of the ^{10}B absorption probability per unit time has been introduced in our COBAYA-87 code[1,2] of detailed (pin-by-pin) two-group diffusion calculation of PWR X-Y average core planes, using the following cell-by-cell accumulation of ^{10}B absorptions:

$$\langle \sigma_a^{10B}\Phi \rangle = \frac{\sum_{i \in R} V_i N_i^{10B} \sum_g \sigma_{ai,g}^{10B} \Phi_{i,g}}{\sum_{i \in R} V_i N_i^{10B}} \tag{5}$$

in terms of the cell volumes, ^{10}B number densities, and microscopic group cross sections and fluxes per cell i and group g. The sum in the numerator extends over all active core and reflector cells, while that in the denominator is restricted to the active core volume, including all fuel and water cells.

For cycle 4 of the C. N. Almaraz PWR, designed for a length very close to 1 yr at rated power, with a low-leakage loading pattern using a moderate number of lumped burnable absorber wet tubes, the calculated core-average ^{10}B absorption probability is ~3.5 to 4.0/yr from beginning to end of cycle. This results, within the continuous boron dilution model and the above mentioned data, in an almost linear reduction of the ^{10}B isotopic abundance in the primary system along the cycle that reaches ~80% of the initial abundance after 1 yr of effective length at full power.

The inverse of the ^{10}B remaining fraction is the correction factor to be applied to the calculated critical boron concentration letdown curve along cycle burnup, with a constant (natural) ^{10}B isotopic abundance. Figure 1 includes the uncorrected (solid line) and corrected (broken line) critical boron letdown curves calculated by the COBAYA-87 code for cycle 4
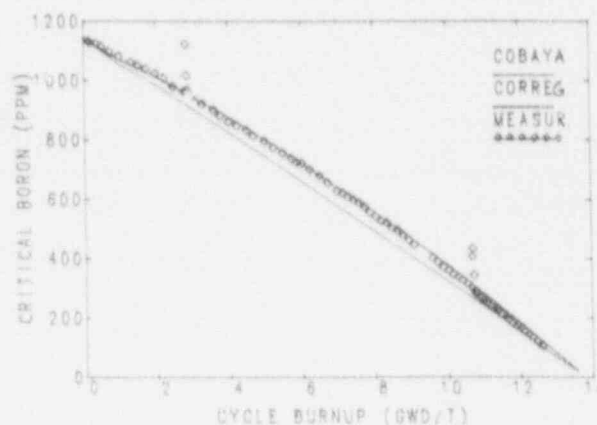

Fig. 1. Boron letdown in cycle 4 of Almaraz-II.

of C. N. Almaraz Unit II, together with a selection of measured values (6) along actual operation up to the present (end of May 1988). Included also are the measured values during the ramps back to rated power in the only two trips that occurred in this cycle. The first trip was early in the cycle when the ^{10}B depletion was still low, so that the effect of the injected borated water was small. In the second, near the end of cycle, the boron concentration was increased by ~40%, and so the ^{10}B isotopic abundance increased from 85 to 89% of the natural one, which resulted in a decrease of ~12 ppm (4% of 300 ppm) in the measured critical boron back to nominal conditions, confirming our model predictions.

In conclusion, the limiting continuous boron dilution model with the ^{10}B depletion calculations based on our COBAYA code is in quite good agreement with the measured boron concentrations for this cycle, explaining very well the differences found with the expected design letdown curve, which increased up to +60 ppm at middle of cycle when this work was done.

1. J. M. ARAGONÉS, C. AHNERT, "The Generalized Synthetic Diffusion Method. Implementations in the SEANAP Code System and Validation for PWR Core Analysis," *Revista de la Sociedad Nuclear Española*, 60, 17, Intl. Issue (Dec. 1987).

2. A. CRESPO, C. AHNERT, J. M. ARAGONÉS, "Pin Power and Burnup Calculations by the SEANAP PWR Core Analysis System," accepted for ANS Reactor Physics Conf., Jackson Hole, Wyoming (Sep. 1988).

The results of this analysis demonstrated the average eigenvalue for all criticals predicted by CASMO-3G to be 0.9954 ± 0.0088. No significant trends with fuel enrichment, soluble boron concentration, buckling, or water-to-metal ratio were noted. The isotopic benchmarks demonstrated CASMO-3G to predict isotopic concentrations to measured data within the measurement uncertainty. The measurements included data up to pin exposures to 52 000 MW/tonne U. No significant trend in the results with exposure was noted. The gamma transport benchmarking demonstrated the code again to be within the uncertainty of the measured data in predicting gamma detector response.

SIMULATE-3

SIMULATE-3 is an advanced nodal code using two explicit energy groups and requiring no normalizations. The code can be used for a broad range of global core model physics licensing calculations in either two or three dimensions.

To validate the code, again, a series of benchmarks was conducted to test the calculational capability of the code. This included a series of established numerical core model benchmarks and comparison to operational data for both PWR and BWR designs.

The calculations included assembly relative power comparisons, critical boron letdown comparisons, detector axial trace comparisons, and comparisons to low-power physics test data.

The results demonstrate SIMULATE-3 predicts radial assembly power versus measured data to <2%, on average. This is within the measurement uncertainty. On start-up physics parameters, critical boron is within 15 ppm, control rod worths are within 3%, and temperature coefficients are <1 pcm/°F. Axial distributions are within 1% of measured data from movable detector traces.

Yankee Atomic is currently evaluating the pin power reconstruction capabilities of SIMULATE-3 using the same philosophy discussed above. Results[8,9] to date indicate the accuracy of this approach to be on the order of our current method.

CONCLUSION/FUTURE WORK

The generic CASMO-3G/SIMULATE-3 benchmarking and verification program at YAEC has demonstrated the applicability of the codes to perform physics analyses for both licensing and steady-state operation. In addition, an experience base has been developed in house for using and understanding the codes and their results. Future comparisons will be made on specific YAEC plants.

The results also demonstrate that the codes perform to the same degree of accuracy or better when compared to our current licensing method. The results using our current licensing method, however, reflect application of known biases based on observation to measured data. The CASMO-3G/SIMULATE-3 results have no bias applied to them as they appear unnecessary.

1. R. J. CACCIAPOUTI, E. E. PILAT, "Physics Methods Verification at Yankee," *Trans. Am. Nucl. Soc.*, **33**, 819 (1979).

2. R. J. CACCIAPOUTI et al., "Benchmarking Lattice Physics Data and Methods for Boiling Water Reactor Analysis," *Proc. Thermal Reactor Benchmark Calculations, Techniques, Results, and Applications*, May 1982, NP-2855, Electric Power Research Institute.

3. A. S. DiGIOVINE, "PURPAS—Program to Upgrade Reactor Physics Analysis Services," YAEC-1616, Yankee Atomic Electric Company (Oct. 1987).

4. M. EDENIUS et al., "CASMO-3G, A Fuel Assembly Burnup Program," Studsvik/NFA-86/7, Studsvik Energitenik (Nov. 1986).

5. D. VerPLANCK, K. S. SMITH, "SIMULATE-3 Manual," Studsvik of America (to be published).

6. W. R. CADWELL, "PDQ-7 Reference Manual," WAPD-TM-678, Westinghouse Bettis Atomic Power Lab. (1967).

7. A. S. DiGIOVINE et al., "CASMO-3G Validation," YAEC-1363, Yankee Atomic Electric Company (Jan. 1988).

8. A. S. DiGIOVINE, D. G. NAPOLITANO, "SIMULATE-3 Pin Power Reconstruction and Comparison to Fine Mesh PDQ-7," *Trans. Am. Nucl. Soc.*, **54**, 361 (1987).

9. A. S. DiGIOVINE et al., "SIMULATE-3 Pin Power Reconstruction Applied to Seabrook Station," *Trans. Am. Nucl. Soc.*, **55**, 590 (1987).

ANS TRANSACTIONS, Vol 56

3. SIMULATE-3 Pin Power Reconstruction: Benchmarking Against the B&W Critical Experiments. *Kord S. Smith (Studsvik USA)*

INTRODUCTION

Efforts to benchmark the accuracy of the SIMULATE-3 nodal code[1-4] with pin power reconstruction fall into three distinct categories. Initial activities concentrated on benchmarking SIMULATE-3, using only single-assembly CASMO-3 data, against CASMO-3 color-set (four-assembly) calculations. This permitted determination of pin power accuracy relative to pin-by-pin multigroup transport calculations. These tests demonstrated[4,5] that accurate pin powers can be reconstructed—even for color sets comprised of assemblies with large differences in enrichment, burnable absorber loadings, and/or exposures. SIMULATE-3 pin power distributions have root-mean-square differences <1.0%, relative to CASMO-3, for both first- and second-cycle (shuffled) depletion color sets.

In a second category of tests, quarter-core PDQ and SIMULATE-3 nodal calculations were compared for several cycles of simulated reactor operation. These tests[5,6] demonstrated that SIMULATE-3 is capable of accurately predicting pin power distributions throughout the core during depletion, and degradation of accuracy has not been observed following core shufflings—where one might expect the pin power reconstruction methods to be least accurate.

Comparisons with several consecutive cycles of measured plant data[7-9] have demonstrated that SIMULATE-3 is capable of predicting instrument thimble reaction rates with ~1.0% accuracy. Such tests are very important, but they provide only limited evidence of pin power accuracy, because reaction rates are measured in the guide tubes at the center of each assembly and actual pin powers are not measured.

Pin-by-pin power distributions have, however, been measured in several critical assemblies,[10,11] and comparisons with such measurements permit direct evaluation of uncertainties in predicted pin power distributions. In this paper, results of SIMULATE-3 pin power reconstruction are presented for the Babcock & Wilcox (B&W) series of urania/gadolinia cores.[11]

THE B&W CORES

In the B&W experiments,[11] critical cores were relatively large (five assemblies in diameter), and a large number of interesting fuel assembly designs were used. The assemblies included low (2.46%) and high (4.02%) enrichments, small (15 × 15 B&W) and large [16 × 16 Combustion Engineering (C-E)] water holes, and heavy gadolinia loadings (16 Gd pin/assembly). Each pin in the central assembly was gamma scanned following irradiation, and three separate irradiations were performed for each configuration. Consequently, statistical uncertainties[11] of the power distributions were quite small (~0.5%).

Code Benchmark and Uncertainties

CASMO-3/SIMULATE-3 MODELS

Three-dimensional SIMULATE-3 models of the B&W cores were constructed using a 2×2 mesh-per-assembly nodal model, which necessitated small compromises to the as-built core geometries. The number of pins that were incorrectly modeled was quite small, and all such pins were located on the core periphery. Furthermore, calculations demonstrated that the central assembly power distributions were insensitive to modeling compromises.

Assembly-homogenized cross sections, discontinuity factors,[2,3] and pin power form functions[4] required by SIMU-

TABLE I

Summary of Errors in SIMULATE-3 Pin Power Distributions
for the Babcock & Wilcox Urania/Gadolinia Cores

Core No.	1	5	12	14	18	20
Fuel Assembly Design	2.46% 15x15 0 Gd	2.46% 15x15 12 Gd	4.02% 15x15 0 Gd	4.02% 15x15 12 Gd	4.02% 16x16 0 Gd	4.02% 16x16 16 Gd
RMS Difference (SIMULATE-3 minus Meas.)	0.6%	1.5%	0.9%	1.2%	0.8%	1.2%
Error in Peak Pin (SIMULATE-3 minus Meas.)	-0.1%	+1.1%	+0.5%	+0.4%	-0.8%	+1.3%
Average Error in Gd Pins	-----	1.9%	-----	2.2%	-----	1.4%

TABLE II

Fission Rate Distributions[a] in Babcock & Wilcox Cores with Combustion Engineering Pressurized Water Reactor Lattice

Core 18: 4.02% Enriched, Large Water Holes with 0 Gd Pins								Core 20: 4.02% Enriched, Large Water Holes with 16 Gd Pins						
WATER	1.205 1.217 +.012	1.033 1.031 -.002	0.997 0.998 +.001	0.997 0.984 +.013	0.959 0.966 +.007	0.941 0.946 +.005	0.909 0.923 +.014	WATER	1.277 1.294 +.017	1.082 1.087 +.005	1.059 1.061 +.002	1.043 1.056 +.013	1.043 1.046 +.003	1.017 1.035 +.018	1.010 1.030 +.020
	1.076 1.079 +.003	1.021 1.031 +.010	1.012 1.025 +.013	1.010 1.012 +.002	0.982 0.981 -.001	0.946 0.949 +.003	0.912 0.919 +.007		1.110 1.114 +.004	1.011 0.999 -.012	1.059 1.060 -.001	1.075 1.077 +.002	1.034 1.036 +.002	0.973 0.959 -.014	0.979 0.999 +.020
		1.065 1.079 +.014	1.228 1.218 -.010	1.203 1.204 +.001	1.043 1.039 -.004	0.957 0.957 +.000	0.928 0.917 -.011			*0.168* *0.165* *-.003*	1.238 1.208 -.030	1.268 1.283 +.015	1.073 1.045 -.028	*0.164* *0.162* *-.002*	0.954 0.938 -.016
				WATER	1.183 1.176 -.007	0.974 0.965 -.009	0.924 0.912 -.012					WATER	1.284 1.263 -.019	0.972 0.982 +.010	0.999 0.994 -.005
					1.170 1.162 -.008	0.970 0.954 -.016	0.909 0.900 -.009						1.280 1.278 -.002	1.045 1.046 +.001	0.999 1.008 +.009
					0.995 1.002 +.007	0.924 0.923 -.001	0.886 0.883 -.003						1.077 1.085 +.008	0.962 0.951 -.011	0.978 0.972 -.006
		Measured SIMULATE-3 S-3 - Meas.	------- ------- -------	0.893 0.891 -.002	0.866 0.863 -.003				Measured SIMULATE-3 S-3 - Meas.	------- ------- -------	*0.158* *0.156* *-.002*	0.900 0.898 -.002
						0.833 0.841 +.008				********** * Gd Pin * **********			0.931 0.933 +.002

[a]Calculated and measured distributions are normalized to unity in the central assembly.

LATE-3 were generated using single-assembly CASMO-3 calculations[12] of each assembly type. Reflector data for SIM-ULATE-3 were generated using the CASMO-3 reflector option,[2,3] and cross sections were tabulated as functions of the boron concentration, fuel temperature, and moderator temperature. In essence, the CASMO-3/SIMULATE-3 models of the B&W cores utilized were the same as those used by the Studsvik code system to analyze power reactors.

RESULTS

SIMULATE-3 pin power distributions were computed for each of the six B&W configurations in which pin-by-pin power distributions were measured. Comparisons of the S. ULATE-3 results to the measured data are summarized in Table I, and detailed pin power distributions are presented for two of the cores in Table II. These results demonstrate that uncertainties in SIMULATE-3 pin powers are ~0.8% in assemblies without gadolinium and 1.3% in assemblies containing gadolinium. Peak power pins, as well as low-power gadolinium pins, are well predicted by SIMULATE-3.

CONCLUSIONS

The calculated pin power distributions in the B&W core provide direct evidence of the high accuracy of CASMO-3/SIMULATE-3 pin powers. Even in the gadolinium cores, which have checkerboard gadolinium loadings, pin powers are very accurately predicted, and similar accuracy is expected in other complicated core loadings. It is also significant that SIMULATE-3 is capable of retaining this accuracy in reactor configurations that have complicated axial loadings and require accurate three-dimensional analysis.

Since the SIMULATE-3 pin power reconstruction method[4] utilizes a modulation of intranodal power distributions with the CASMO-3 single-assembly (infinite lattice) power distributions, the high accuracy of the SIMULATE-3 pin powers also implies that CASMO-3 very accurately predicts pin-by-pin power distributions in all types of lattices, including the C-E lattice and/or gadolinium-bearing assemblies.

1. K. S. SMITH, D. M. VerPLANCK, M. EDENIUS, "QPANDA: An Advanced Nodal Method for LWR Analyses," Trans. Am. Nucl. Soc., 50, 532 (1985).

2. M. EDENIUS, K. S. SMITH, D. M. VerPLANCK, "Recent Developments in the MICBURN/CASMO/SIM-ULATE LWR Analysis Package," presented at ANS Topl. Mtg. Advances in Fuel Management, Pinehurst, North Carolina, 1986.

3. M. EDENIUS, K. S. SMITH, D. M. VerPLANCK, "New Data and Methods for CASMO and SIMULATE," ANS Topl. Mtg. Reactor Physics and Safety, Saratoga Springs, New York, 1986.

4. K. S. SMITH, K. R. REMPE, "Testing and Applications of the QPANDA Nodal Model," Proc. Int. Mtg. Advances in Reactor Physics, Mathematics, and Computation, Paris, France, 1987, Vol. II, p. 861 (1987).

5. A. S. DiGIOVINE, D. G. NAPOLITANO, "SIMU-LATE-3 Pin Power Reconstruction and Comparison to Fine-Mesh PDQ," Trans. Am. Nucl. Soc., 54, 361 (1987).

6. A. S. DiGIOVINE et al., "SIMULATE-3 Pin Power Reconstruction Applied to Seabrook Station," Trans. Am. Nucl. Soc., 55, 590 (1987).

7. K. REMPE, K. SMITH, "SIMULATE-3 Power Distributions and Detector Response Modeling," Trans. Am. Nucl. Soc., 54, 355 (1987).

8. A. S. DiGIOVINE et al., "CASMO-3/SIMULATE-3 Benchmarking Against McGuire Unit 2," Trans. Am. Nucl. Soc., 55, 591 (1987).

9. K. S. SMITH et al., "SIMULATE-3 PWR Benchmark Report, Farley Unit II," STUDSVIK/SOA-87-10, Studs-vik of America (1987).

10. R. PERSSON, E. JOHANSSON, "KRITZ Critical Experiments," Personal Communication (1987).

11. L. W. NEWMAN, "Urania-Gadolinia: Nuclear Model Development and Critical Experiment Benchmark," DOE/ET/34212-41, BAW-1810, Babcock & Wilcox (1984).

12. M. EDENIUS et al., "CASMO-3 A Fuel Assembly Burnup Program," STUDSVIK/NFA-86/8, Studsvik of America (1986).

4.   Analysis of Gadolinium Depletion Measurements with the TGBLA BWR Lattice Physics Method, *Koichi Sakurada, Tomio Tanzawa, Munenari Yamamoto (NAIG–Japan), Ritsuo Yoshioka (Toshiba IEC–Japan), invited*

INTRODUCTION

Irradiation experiments of poison rods with high-concentration gadolina (up to 9 wt% Gd_2O_3) have been performed to obtain the benchmark data on the depletion of gadolinium isotopes with burnup and the radial distribution of gadolinium isotopes in the poison pellet. A detailed description of the experimental procedure and results were reported in Ref. 1.

In the present study, the analyses of irradiation experiments have been carried out using the boiling water reactor (BWR) fuel nuclear design code TGBLA (Ref. 2) to testify to the validity of its methods.

EXPERIMENTAL DATA

The following experimental procedure and results were obtained from Ref. 1. Three test assemblies were irradiated in the Halden BWR, each of which consists of 3×3 fuel rods arranged in a square lattice cluster with a 16-mm rod pitch. The center rod is a Gd_2O_3 poison rod, which is composed of two segments that have 6 and 9 wt% Gd_2O_3 in UO_2 pellets.

Nondestructive postirradiation examinations were performed on the mass-spectrometry measurements of fuel burnups, pellet average isotopic concentrations, and radial distributions of gadolinium, uranium, plutonium, and neodymium isotopes in poison pellets.

METHOD OF CALCULATIONS

Analyses of the irradiation experiments were performed with the TGBLA code, which had been developed for the use of BWR lattice design calculations in a cooperative study between Toshiba Corporation and General Electric Company. The TGBLA cross-section library consists of the THERMOS-type 30-group library and the GAM-type 68-group library, both of which are generated from the ENDF/B-V file for the main heavy nuclides and the JENDL-2 file for the fission product nuclides.

The treatment of the poison rod is especially important to calculational accuracy for BWR fuels with gadolinium-bearing rods. Each poisoned rod is divided into multiannular burn regions to stimulate the "onion-skin" depletion of gadolinium isotopes. The same treatment is adopted in the thermal neutron spectrum calculations to account for the significant spatial variation of the thermal neutron spectrum inside poison pellets.

RESULTS AND COMPARISONS

A comparison was made between the calculational and experimental results of the following quantities:

NUCLEAR SCIENCE AND ENGINEERING®

(ISSN: 0029-5639)

THE RESEARCH JOURNAL OF THE AMERICAN NUCLEAR SOCIETY

PARIS PAPER   M. Edenius

"CASMO-3: NEW FEATURES, BENCHMARKING, &
ADVANCED APPLICATIONS"

CASMO-3: New Features, Benchmarking, and Advanced Applications

Malte Edenius

Studsvik of America, Inc., 1087 Beacon St., Suite 301, Newton, Massachusetts 02159

and

Ake Ahlin

Studsvik Energiteknik AB, S-61182 Nykoping, Sweden

Abstract — *The CASMO code is an assembly spectrum code that uses multigroup integral transport theory with four thermal energy groups for the two-dimensional calculation. The latest version, CASMO-3, contains several new features, specifically a new data library, multibundle capability, gamma detector calculation, flux discontinuity factor edit, and an option for generating transport theory corrected baffle/reflector data. Extensive benchmarking, including comparisons against cold- and high-temperature critical experiments, Monte Carlo calculations, measured isotopics, and power reactor core follow, has verified that accurate results are obtained. The new multibundle capability has been used for studies of interassembly spectrum coupling and for validation of core physics methods.*

INTRODUCTION

The CASMO code is currently used by about 40 utilities worldwide as a tool incorporated with code packages for reactor operating support, bundle and core design, licensing, safety analysis, and scoping studies. It is also being used by fuel vendors, licensing authorities, consultants, and research laboratories.

This paper gives an overview of the CASMO development and specifically explains new features in the latest version of the program, CASMO-3 (Ref. 1).

HISTORY OF CASMO DEVELOPMENT

One-dimensional integral transport theory methods, now used for pin cell homogenization in CASMO, were developed at Studsvik by Carlvik[2] in the 1960s. These methods were incorporated into a heavy water cluster code and a first generation light water reactor (LWR) assembly code by Ahlin and Jonsson[3] in the late 1960s. At that time, several general concepts and the first data libraries were obtained from the development of the WIMS code[4] at Winfrith. The cluster code development and early LWR work were important when a two-dimensional S_4 theory module, SFINX (Ref. 5), was put into an LWR assembly code at Studsvik in 1969–70.

Although the early CASMO development benefited from the cluster code and the first LWR assembly code, CASMO has retained only Carlvik's integral transport theory and the WIMS energy group boundaries of the data library. The S_4 module was replaced by a more accurate transmission probability module, COXY (Ref. 6), in the mid-1970s and all other parts of the earlier code were replaced by new methods before the first CASMO version[7] was released in 1976. The original CASMO data library[8] was based on ENDF/B-III. The CASMO code has since been used for LWR assembly calculations without changes in data or methodology until the recent introduction of CASMO-3.

EARLIER CASMO VERSIONS

Versions 1, 2, and 2E of CASMO use the same physics model and data library, and they differ only in the availability of more options in the later versions. A flowchart of the calculational sequence is similar to that of many other assembly codes. Only a few specific features that are of major importance for the quality and flexibility of the code are discussed below.

Two-Dimensional Integral Transport Theory

Early in the development of CASMO it was found that diffusion theory is inadequate for the accuracy we desired in the two-dimensional assembly calculation. The S_4 theory was found to be superior to diffusion theory but less accurate than the collision probability method used in EPRI-CPM (Ref. 9), which was developed by Studsvik for Electric Power Research Institute. The collision probability method has a disadvantage in being sensitive to mesh size.[10] Typically 3×3 meshes per pin cell are needed to obtain accurate results, and such computations require too extensive computer resources to be used for large volume production of few-group data.

The choice for CASMO is the transmission probability COXY model,[6] which we found to be superior to the above-mentioned methods. The COXY model is more accurate[6,10] than any of the other models but is still very computer efficient.

In COXY, the current due to transmission of neutrons from one mesh boundary to another boundary and to escape of neutrons from the inner part of the mesh is calculated. Transmission and escape probabilities are calculated exactly for the homogeneous rectangular meshes but approximations are made for the spatial and angular expansion of the currents and for the source distribution within the mesh. Because COXY accounts for a linear variation of the flux within each mesh, the results are extremely insensitive to the mesh size.

Four Two-Dimensional Thermal Energy Groups

The thermal spectrum in an LWR assembly with water gaps or water holes and with absorber rods varies drastically for different locations within the assembly. We therefore found it necessary to use several thermal energy groups in the two-dimensional calculation. The CASMO code allows more energy groups, but four thermal and three epithermal groups were found to be adequate for all fuel types existing today. The use of a smaller number of energy groups would, however, result in a loss of accuracy in the calculated power next to water holes or absorbers due to the rapid change of spectrum in the vicinity of the heterogeneities.

With the computational speed achieved by COXY, there is no reason to give up accuracy by decreasing the number of energy groups, and, because of the insensitivity of the method to mesh size, the user always obtains "well converged" results versus number of energy groups and mesh size.

THE MICBURN GADOLINIUM DEPLETION MODEL

For gadolinium depletion calculations, CASMO uses the well-proven MICBURN methodology[11] to calculate the microscopic burnup within a pellet. It has been demonstrated[12] that the details of the microscopic burnup are not needed for nonpoisoned fuel pins but are essential for the gadolinium pins. The MICBURN methodology uses a "traditional" simplified geometry where the gadolinium pin cell is modeled in great detail (with typically 20 to 30 radial depletion zones within the pellet), but the surrounding environment is simplified by a circular buffer zone.

The strength of MICBURN comes from the fact that the smearing of output data is done only for the fuel pellet (not for the whole pin cell) and that no energy condensation is done in MICBURN. This results in gadolinium cross-section tables for CASMO that are essentially independent of the environment, enrichment, temperature, etc. Therefore, it is easy to tabulate the effective gadolinium cross sections, and the user only needs to run MICBURN for new types of gadolinium pellets, e.g., a new annular design.

Thus, MICBURN serves two purposes. First, MICBURN allows a more detailed depletion, shorter time steps, and more spatial detail, than what would be feasible if the detailed gadolinium depletion needed to be redone within CASMO for each assembly depletion. Second, computer resources are saved because the detailed gadolinium depletion is done only once for each type of gadolinium rod.

The current MICBURN version, MICBURN-3 (Ref. 13), differs from earlier versions only in added flexibility, e.g., microscopic depletion calculations on fuel without gadolinium to determine the radial power and exposure distribution within the pellet. The MICBURN-3 code also handles gadolinium in annular pellets and other types of burnable poison rods (BPRs), e.g., rhodium detectors, etc.

The MICBURN-3Z version[14] allows the analysis of grey gadolinium rods consisting of Gd_2O_3-UO_2 pellets mixed with regular UO_2 pellets. This calculation is done in r-z geometry.

It is important for a proper gadolinium depletion that the complete gadolinium chain from ^{154}Gd to ^{158}Gd be included. (There are also small contributions from ^{152}Gd and ^{160}Gd.) Before the development of MICBURN, CASMO was frequently used with gadolinium data generated from a Monte Carlo program,[15] FOBUS, which today is not recommended because it lacks the proper depletion chains. The Monte Carlo methodology also has the disadvantage

of very long running times and statistic uncertainties that are avoided with MICBURN.

CASMO-2E

Some additional features of CASMO-2E, all of which are retained in CASMO-3, are discussed below.

Macroscopic and microscopic cross sections can be edited for use in fine-mesh PDQ core calculations. The CASMO code also contains a two-dimensional diffusion theory module that is used to verify whether few-group diffusion theory reproduces the accurate multigroup transport theory results. An iterative technique allows cross sections to be changed in the diffusion theory calculation until agreement is achieved and the cross-section correction factors, called G-factors in PDQ, are edited[16] by CASMO.

The flexibility of CASMO is demonstrated by the fuel storage rack capability, which allows extra slab regions around the bundle for rack criticality studies.[17] The deterministic transport method in CASMO has several advantages compared to more conventional Monte Carlo calculations for criticality studies. Computer and manpower requirements are drastically reduced, and sensitivity studies for dimensional or material variations are easily done without disturbing statistical uncertainties.[18]

The auxiliary MOVEROD allows burnt fuel pins to be shuffled within a bundle or moved from one bundle to another.

NEW FEATURES IN CASMO-3

New Data Library

One important change in CASMO-3 is the new data library,[19] which contains cross-section data based on ENDF/B-IV and -V in 70 energy groups. A condensed 40-group library is normally used for production calculations, because it saves some computer time without any loss of accuracy (unless the user, for very special applications, needs the more detailed 70-group spectrum).

Multibundle Capability

Earlier CASMO versions were limited to single-bundle calculations, which are adequate for most types of few-group cross-section generation. There are, however, certain investigations that require a larger geometry, and CASMO-3 was therefore extended to treat 2 × 2 boiling water reactor (BWR) bundles or a pressurized water reactor (PWR) color sets (four quarter bundles). Mirror, rotational, and periodic boundary conditions can be used, and the input allows easy shuffling of burnt bundles between both single- and multibundle CASMO runs.

Gamma Detector Calculation

Gamma sensitive detectors are used today in both BWRs and PWRs. The CASMO-3 code generates the gamma detector response by use of a 10- or 18-group gamma transport calculation that is carried out with the same transmission probability routine as is used for the neutron transport calculation. Separate transport calculations can be performed for the prompt and delayed gamma sources. The method is similar to that developed[20,21] for CASMO-1 and CPM except for the use of COXY instead of CPM for the two-dimensional calculation.

Flux Discontinuity Factors

For the past few years, significant progress has been made in the development of two-group nodal codes, e.g., the QPANDA model[22,23] used in Studsvik's SIMULATE-3,[24,26] with a theoretical model that does not require normalizations against higher order calculations or measurements. The SIMULATE-3 code uses flux discontinuity factors for bundle surfaces to predict correct net currents between bundles. The CASMO-3 code calculates the two-group flux discontinuity factors for each surface in both single- and multibundle calculations.

Reflector Calculations

Furthermore, the new advanced nodal codes use explicit reflector representation instead of albedos. This requires a consistent method for the calculation of homogenized two-group baffle/reflector data. In CASMO-3, a model was developed that generates few-group cross sections for baffle and reflector water, as well as for any homogenized baffle/reflector region.[25] The use of flux discontinuity factors on the reflector boundaries preserves CASMO's multigroup transport theory leakage when the two-group cross-section data are used in core calculations.

The CASMO-3 code also generates four-group reflector data including four-group discontinuity factors for use in PDQ or other diffusion theory codes. The same model is used for generation of axial reflector data.

New Fuel Designs

The CASMO-3 code can handle all existing LWR bundle designs, including SVEA (or Quad+) and 9 × 9 BWR bundles with large square-shaped or annular water rods, hybrid control blades containing both boron carbide (B_4C) and zones, boron-coated fuel pellets, etc.

BENCHMARKING

The new data library and modifications in the CASMO-3 model have necessitated extensive new

CASMO-3   345

benchmarking.[27,28] The wide range of critical experiments covered were (a) pin cell lattices, (b) BWR lattices with and without absorbers, (c) PWR lattices with small and large water holes and absorbers, and (d) storage rack configurations with large water gaps.

The parameters that were compared to measured data include

1. k_{eff} versus temperature, ^{235}U enrichment, plutonium concentration, water-to-fuel ratio, boron concentration, leakage, water gap thickness, gadolinium, B_4C, silver-indium-cadmium, and cruciform control rod absorption

2. fission rate distributions in BWR and PWR assemblies at hot temperatures with and without absorbers.

It is essential that the critical benchmarks include this wide variety of lattices and the hot temperature criticals, namely, the KRITZ experiments up to 245°C. This permits verification of both data and methodology, including the two-dimensional transport theory model and absorber calculations.

Calculated k_{eff} values[27] (Table I) show no trend versus any of the investigated parameters. The k_{eff} statistical result (which is frequently quoted in pin cell code benchmarks) for the cold pin cell lattices, including ESADA MO_2 cores, is $k_{eff} = 1.0002 \pm 0.0010$. A more stringent test of an assembly code's accuracy needs to include hot temperature cores and assemblies with and without absorbers. For all calculated cores (37 cases), CASMO-3 predicted $k_{eff} = 1.0004 \pm 0.0011$.

The root-mean-square (rms) error in calculated

TABLE I

CASMO-3 Calculated k_{eff} for Criticals

Core		k_{eff}	
		Cold	Hot
Pin cell cores			
BAPL T6	1.31% enriched	1.0013	---
KRITZ-1	1.35	0.9987	0.9988
KRITZ-2.1	1.9 $V_m/V_f = 1.2$	1.0000	1.0007
KRITZ-2.13	1.9 $V_m/V_f = 1.7$	0.9989	0.9990
B&W B20	2.46	1.0008	---
ESADA-1	2.0% PuO_2 (8% ^{240}Pu)	0.9994	---
ESADA-20	2.0% PuO_2 (24% ^{240}Pu)	1.0008	---
KRITZ-3 PWR cores			
U-WH1	Small water holes	0.9988	0.9993
U-CR1	Silver-indium-cadmium control rods	1.0003	0.9988
U-WH2	Large water holes	1.0003	1.0002
U-CR2	Large B_4C control rods	0.9997	0.9995
KRITZ-4 BWR cores			
Wide gap at core center			
2.1	No gadolinium	1.0006	---
2.2	No gadolinium, with control rod	1.0002	---
2.5	Seven gadolinium rods/bundle	1.0001	---
Narrow gap at core center			
3.1	No gadolinium	1.0010	1.0016
3.2	Five gadolinium rods/bundle	1.0016	1.0015
3.5	Three gadolinium rods/bundle	1.0018	1.0015
Checker board loading			
4.1	No gadolinium—five gadolinium bundles	1.0007	1.0004
4.2	No gadolinium—three gadolinium bundles	1.0013	---
All gadolinium bundles			
5.1	Three gadolinium rods/bundle	1.0003	0.9993
Storage rack configurations			
B&W I	No gap, 0 ppm B	1.0003	---
B&W II	No gap, 1037 ppm B	1.0015	---
B&W III	1.63-cm gap	1.0029	---
B&W X	4.89-cm gap	1.0024	---
B&W IX	6.52-cm gap	1.0004	---

346   EDENIUS and AHLIN

fission rate distributions is ~1%, i.e., the same as the experimental uncertainty, for both PWR and BWR assemblies with and without gadolinium. Figures 1 and 2 show results for a BWR assembly with five gadolinium rods and for a Combustion Engineering assembly with large water holes. In total, some ten different high-temperature fission rate distributions were analyzed and no trend could be observed for pins around water holes, along water gaps, in corner positions, in gadolinium rods or around absorbers.

Other data used for benchmarking include (a) Hellstrand's resonance integral and Doppler coefficient measurements for ^{238}U, (b) epithermal-to-thermal reaction rate ratios, (c) numeric benchmarks with Monte Carlo calculations, (d) uranium and plutonium isotopics in burnt fuel, and (e) BWR and PWR core follow using CASMO-3 cross sections. The resonance integrals and Doppler coefficients shown in Table II all agree well within the experimental uncertainties.

Epithermal-to-thermal reaction rate ratios for the triggered reconnection experiment (TRX) and Bettis Atomic Power Laboratory pin cell benchmarks are listed in Table III. These experiments are simple, cold uniform pin cell lattices without the heterogeneity and complexity of the KRITZ critical experiments. They do, however, provide more details on individual reaction rates, and they are used widely for benchmarking of pin cell codes. We therefore included these experiments in the CASMO-3 benchmarking, and the agreement between CASMO-3 and measurements is excellent.

Table III also shows results for two numeric benchmark problems, NB-1 and NB-4, provided by Oak Ridge National Laboratory. The CASMO-3 results are here compared to Monte Carlo results[29] using SAM-CE and PX-KENO with ENDF/B-V cross sections. Calculated k_{inf} values also agree well between CASMO-3 and Monte Carlo with CASMO giving k_{inf} equal to 1.1454 and 1.3399 and Monte Carlo 1.1471 ± 0.0014 and 1.3424 ± 0.0026 for NB-1 and NB-4, respectively.

Water					
0.978	1.004	-	-	-	-
1.005	-	0.989	-	-	-
-	-	-	Water		
0.966	-	1.011			
1.008	-	0.995	-	1.006	-
1.002	-	-	-	-	1.014

Fig. 1. Ratios of calculated-to-measured fission rates in a 14 × 14 PWR assembly with large water holes. The rms is 0.010.

1.002	-	0.998	-	1.014	-	1.017	-
-	1.002	-	Gadolinium	0.980	-	-	-
-	-	0.978	0.989	-	0.986	-	-
-	Gadolinium 0.999	-	-	-	-	Gadolinium 1.008	0.989
1.021	-	-	1.000	-	0.997	-	-
-	-	-	-	-	-	0.973	-
-	1.016	-	Gadolinium	-	-	Gadolinium 0.999	0.994
1.024	-	1.010	1.003	-	-	-	-

Fig. 2. Ratios of calculated-to-measured fission rates in an 8 × 8 BWR with gadolinium. Ratios are shown for all pins in which measurements were performed. The rms is 0.014.

TABLE II

Comparisons to Experimental ^{238}U Resonance Integrals

	Pellet Radius (cm)	Resonance Integral		Doppler Coefficient	
Fuel		Experiment (b)	C3/Experiment − 1 ($\%$)	Experiment $\ast 100$	C3/Experiment − 1 ($\%$)
UO₂	0.40	23.7	+0.1	0.82	+0.6
	0.52	21.4	−0.4	0.76	+3.5
	0.80	18.4	+0.4	0.70	−2.1
	1.04	16.8	0.0	0.67	−0.2
	1.60	14.6	−0.8	0.64	−0.9
Uranium metal	0.50	16.6	−4.2	0.62	+4.8
	1.00	13.0	−1.0	0.56	−4.8

TABLE III

Summary of Reaction Rate Comparisons

Lattice	ρ_{28}^a	δ_{25}^b	δ_{28}^c	$C^{\ast d}$	k_{∞}
			Experiment		
TRX-1	1.320	0.099	0.095	0.797	---
TRX-2	0.837	0.061	0.069	0.647	---
T6	1.39	0.084	0.078	---	---
T7	1.12	0.068	0.070	---	---
T8	0.906	0.052	0.057	---	---
NB-1	1.363	0.080	0.072	0.798	1.1471
NB-4	2.654	0.159	0.052	0.549	1.3424
			(C3/Experiment − 1) $\ast$ 100		
TRX-1	0.4 (1.6)^e	1.0 (1.0)	4.5 (4.3)	−1.8 (1.0)	---
TRX-2	−0.4 (1.9)	0.0 (1.3)	2.0 (5.0)	−2.0 (0.9)	---
T6	−0.7 (0.7)	0.1 (2.4)	−0.5 (5.1)	---	---
T7	2.9 (0.9)	1.0 (1.5)	−4.4 (5.7)	---	---
T8	0.0 (1.1)	1.5 (1.9)	−3.7 (5.3)	---	---
NB-1	−1.5 (0.6)	2.2 (1.1)	1.9 (0.6)	−1.6 (0.4)	−0.15 (0.14)
NB-4	0.8 (0.6)	−0.1 (0.6)	3.0 (0.8)	−1.3 (0.4)	−0.19 (0.26)

^{a}Epithermal-to-thermal ^{238}U capture.
^{b}Epithermal-to-thermal ^{235}U fission.
$^c{}^{238}U$ to ^{235}U fission.
$^d{}^{238}U$ capture to ^{235}U fission.
^{e}Here, 1σ experimental uncertainties are shown in parentheses.

Comparisons[28] against Yankee Rowe isotopics data are also within the experimental uncertainty. Figure 3 shows the calculated and measured ^{239}Pu to ^{238}U atomic number density ratio versus burnup, and Fig. 4 shows all plutonium isotopes.

Figures 5 and 6 display boron letdown curves for four cycles in a PWR as calculated by CASMO-3/SIMULATE-3. Cycles 1 and 4 contain a large number of BPRs in the fresh fuel. Cycle 2 did not contain BPRs and cycle 3 has BPRs inserted in both fresh and burnt assemblies. Cycle lengths varied from 10 to 16 MWd/t and core average exposure goes from 0 to 25
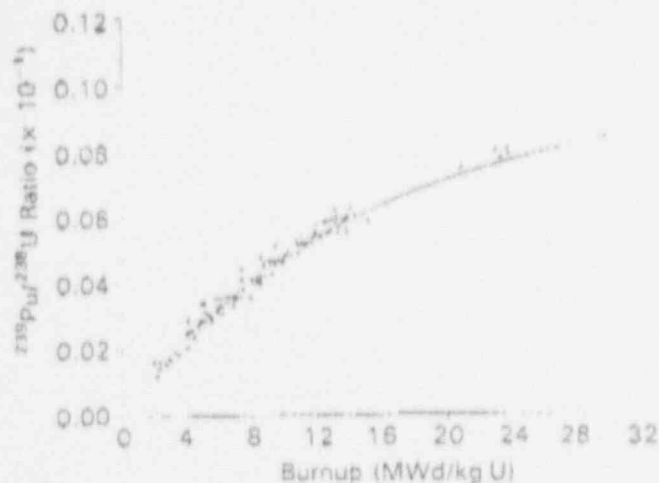
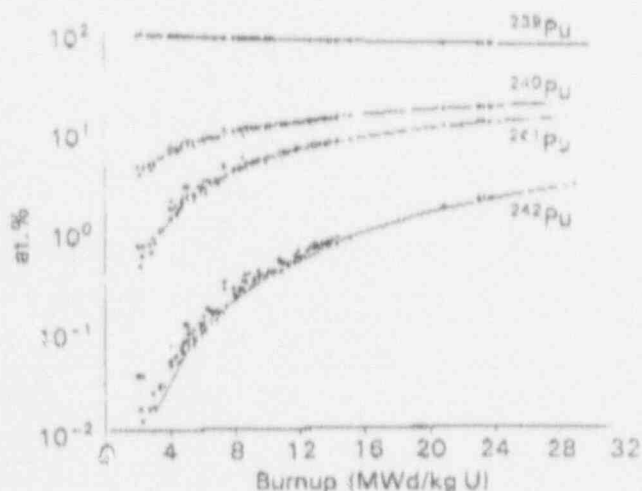Fig. 3. Comparison between calculated and measured ^{239}Pu to ^{238}U atomic ratio versus burnup.

Fig. 5. Calculated and measured boron letdown curves for cycles 1 and 2.

Fig. 4. Comparison between calculated and measured plutonium concentrations versus burnup.
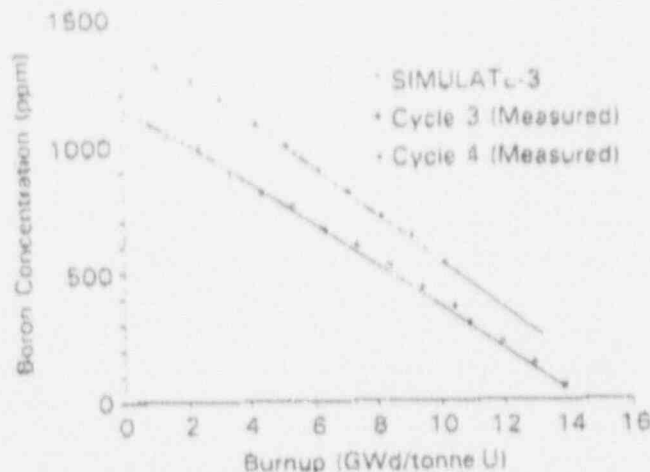
Fig. 6. Calculated and measured boron letdown curves for cycles 3 and 4.

MWd/kg. No trend in boron (k_{eff}) versus burnup can be noticed.

Improvements in CASMO-3 compared to earlier CASMO versions are noticed in the calculated moderator temperature and Doppler coefficients, the leakage, plutonium isotopic concentrations, and k_{eff} versus burnup.

EXAMPLES OF SPECIAL APPLICATIONS

Boron-Coated Fuel

Fuel pellets coated with boron as an integral burnable absorber is a new concept for PWRs. The CASMO code has the flexibility to model the boron smeared into the fu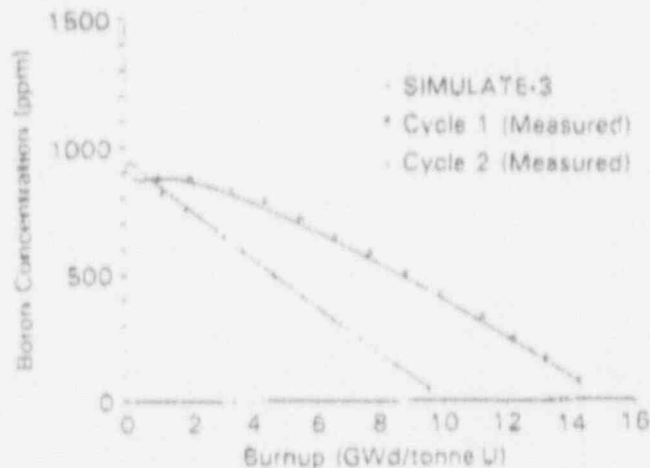el, or into the canning, or as an explicit thin ring around the fuel. The coating on the outside of the pellet is a grey absorber located in a relatively steep flux gradient, and a recent study with CASMO demonstrated that the beginning of life boron worth and the boron depletion rate are overpredicted by 3% if the boron is smeared into the canning, and smearing into the fuel leads to serious underprediction of the worth. This study clearly demonstrated the need to model the coating as an explicit region in both the transport and burnup calculation as is done in CASMO-3.

Gamma and ^{235}U Traveling In-Core Probe Responses for a BWR

It is common to neglect the perturbation of the detector and its surrounding tubes in BWR analyses.

This is done because only 25% of the assemblies are located adjacent to a detector tube and the assemblies are shuffled between every cycle making it a formidable task to account in detail for the detector perturbation. The CASMO code can, however, calculate detector responses with or without the detector present in the calculation.

Table IV compares CASMO calculations with and without the detector structure material included in the model. The gamma traveling in-core probe (TIP) response increased by 5.3 and 2.8% at 0 and 70% void, respectively, while the ^{235}U fission rate in the detector decreased by 19.3 and 20.5% for the two void fractions. The void dependence given in the last column differs, however, by only 2.4 and -1.0% for the gamma and ^{235}U detectors, respectively. In most applications, this is an acceptable error that simplifies the analysis. It is, however, easy for the user to include the detector in the CASMO runs if desired.

Multibundle Calculations

Most CASMO calculations are single-bundle depletions with branch calculations for temperature, boron and void coefficients, and for control rods, etc., at various burnups for generation of complete inputs to core calculations. Such CASMO runs are made on a routine basis in one or several executions at the user's option.

The 2 × 2 BWR option is useful, e.g., for modeling a misloaded (rotated) bundle in a BWR loading, and the PWR color set option allows accurate modeling of, for example, designs with gadolinium rods on the periphery of the bundle, where regular boundary

TABLE IV

Gamma and ^{235}U TIP Responses With and Without Explicit Representation of the Detector

Model	0% Void		70% Void		V70/V0	
	^{235}U	Gamma	^{235}U	Gamma	^{235}U	Gamma
No detector	0.334	0.327	0.309	0.378	0.925	1.155
Explicit detector	0.268	0.345	0.245	0.389	0.916	1.127
Differential (%)	-19.3	$+5.4$	-20.5	$+2.8$	-1.0	-2.4

TABLE V

CASMO-3/SIMULATE-3 Comparison for a First Cycle Depletion of 2 × 2 BWR Segments

Exposure (MWd/kg)	k_∞		Power Distribution			
	CASMO-3	SIMULATE-3	CASMO-3		SIMULATE-3	
0	0.9880	0.9891	0.954	1.022	0.961	1.020
			1.022	1.003	1.020	1.003
2	1.0099	1.0098	0.937	1.028	0.927	1.028
			1.028	1.008	1.028	1.017
4	1.0363	1.0362	0.877	1.042	0.875	1.041
			1.042	1.038	1.041	1.043
7	1.0676	1.0669	0.804	1.059	0.809	1.057
			1.059	1.078	1.057	1.077
10	1.0539	1.0541	0.786	1.063	0.794	1.061
			1.063	1.088	1.061	1.084
12.5	1.0280	1.0287	0.792	1.061	0.797	1.060
			1.061	1.086	1.060	1.083

Segment configuration (enriched/gadolinium rods)   1.1/0   2.5/7
40% void in all segments
No control rods   2.5/7   2.5/7

350   EDENIUS and AHLIN

conditions in a single-bundle calculation would give erroneous results. Furthermore, several studies have been carried out on 2 × 2 BWR configurations as well as PWR color sets for comparisons to single-bundle calculations and to PDQ or SIMULATE-3. Two examples are shown below.

As an example, Table V shows a comparison between CASMO-3 and SIMULATE-3 for a 2 × 2 BWR depletion of a first cycle with islands of low enriched bundles surrounded by high enriched assemblies with heavy gadolinium loading (seven rods containing 4% Gd_2O_3). It can be seen that SIMULATE-3, which used cross sections and discontinuity factors generated in single-bundle CASMOs, is able to reproduce CASMO's k_{eff} and power distribution despite the very large flux gradients that are present in this fairly extreme case.

Table VI shows results for a color set at beginning of cycle in an initial PWR core with large mismatch in enrichment and BPR loading. The CASMO-3 code provides a reference solution from the multigroup transport theory calculation (COXY). Comparisons are then made to the fine-mesh diffusion theory solution (DIXY), also obtained within CASMO-3. The DIXY solution is in this nonburnup application identical to PDQ. The results show that a fine-mesh PDQ calculation in this case overpredicts the power in the BPR bundles by 2% and underpredicts the power in the high enriched bundle by 3%. The G-factors were used in DIXY to generate the correct absorption rate in the BPRs, and this example demonstrates that the use of G-factors does not necessarily result in accurate power distributions in PDQ models.

CONCLUSIONS

The CASMO-3 benchmarking demonstrates the high level of accuracy that is achieved with the new nuclear data and multigroup transport theory. New capabilities, like the generation of discontinuity factors and reflector data, allow the accuracy of CASMO to

be reproduced in core calculations using advanced nodal codes like SIMULATE-3.

The four bundle capability in CASMO-3 can be used for generation of few-group cross sections, discontinuity factors, detector constants, etc. It is also an excellent tool for testing nodal and fine-mesh calculational models.

REFERENCES

1. M. EDENIUS and A. AHLIN, "CASMO-3 User's Manual," STUDSVIK/NFA-86/7, Studsvik (1986).

2. I. CARLVIK, "A Method for Calculating Collision Probabilities in General Cylindrical Geometry," AE-279/P681, Studsvik (1967).

3. A. AHLIN and A. JONSSON, Studsvik, Private Communication (Nov. 1964).

4. J. R. ASKEW, F. J. FAYERS, and P. B. KEMSHELL, J. Br. Nucl. Energy Soc., 5, 564 (1966).

5. R. STAMMLER, "Two-Dimensional S_n Calculations," IAEA Symp. Analytical Methods in the Nuclear Fuel Cycle, Vienna, Austria, November 29–December 3, 1971.

6. H. HÄGGBLOM, A. AHLIN, and T. NAKAMURA, Nucl. Sci. Eng., 56, 411 (1975).

7. A. AHLIN, M. EDENIUS, and H. HAGGBLOM, "CASMO, A Fuel Assembly Burnup Program," AE-RF-76-4158, Studsvik (1976).

8. M. EDENIUS, K. EKBERG, and H. HAGGBLOM, "CASMO, The Data Library," STUDSVIK/K2-81/491, Studsvik (1981).

9. A. AHLIN and M. EDENIUS, The Collision Probability Module EPRI-CPM, Part II, Chap. 6, EPRI-CCM-1, Electric Power Research Institute (1978).

10. M. EDENIUS, Trans. Am. Nucl. Soc., 35, 542 (1980).

11. A. AHLIN and M. EDENIUS, Trans. Am. Nucl. Soc., 41, 594 (1982).

12. M. EDENIUS, Trans. Am. Nucl. Soc., 26, 602 (1977).

13. M. EDENIUS, A. AHLIN, and C. GRAGG, "MICBURN-3, Microscopic Burnup in Burnable Absorber Rods," STUDSVIK/NFA-86/26, Studsvik (1986).

14. C. GRAGG, "MICBURN-3Z, Microscopic Burnup, Radially and Axially, in Burnable Absorber Rods," STUDSVIK/NFA-86/27, Studsvik (1986).

15. G. FREDIN, "FOBUS," Internal Report, AB Atomenergi, Studsvik (1969).

16. A. AHLIN and M. EDENIUS, Trans. Am. Nucl. Soc., 41, 611 (1982).

TABLE VI

COXY/DIXY (CASMO-3/PDQ) Comparison
for PWR Color Set

k_{eff}		Power Distribution			
COXY	DIXY	COXY		DIXY	
1.0287	1.0306	0.880	0.877	0.884	0.895
		0.877	1.364	0.895	1.323
Segment configuration (enriched/BPRs):		1.6/0	2.4/24		
		2.4/24	3.1/0		

CASMO-3   531

17. M. EDENIUS et al., "CASMO Benchmarking Against Critical Experiments in Rack Geometries," STUDSVIK/NR-81/51, Studsvik (1981).

18. D. G. NAPOLITANO, D. P. HEINRICHS, and J. P. GORSKI, *Trans. Am. Nucl. Soc.*, 53, 300 (1986).

19. H. HAGGBLOM, "The CASMO-3 Data Library," STUDSVIK/NFA-86/12, Studsvik (1986).

20. A. AHLIN, M. EDENIUS, S. SUK, D. R. HARRIS, and D. OZER, *Trans. Am. Nucl. Soc.*, 47, 434 (1984).

21. M. EDENIUS, P. J. RASHID, D. M. VER PLANCK, and O. OZER, *Trans. Am. Nucl. Soc.*, 49, 431 (1985).

22. K. S. SMITH, D. M. VER PLANCK, and M. EDENIUS, *Trans. Am. Nucl. Soc.*, 50, 532 (1985).

23. K. SMITH and K. REMPE, "Testing and Applications of the QPANDA Nodal Model," Int. Topl. Mtg. Advances in Reactor Physics, Mathematics, and Computations, Paris, France, April 27-30, 1987.

24. D. M. VER PLANCK et al., "SIMULATE-3 Users Manual," Studsvik/SOA-86/8, Studsvik (1986).

25. M. EDENIUS, K. SMITH, and D. M. VER PLANCK, "Recent Developments in the MICBURN/CASMO/SIMULATE LWR Analysis Package," *Proc. Topl. Mtg. Advances in Fuel Management*, Pinehurst, North Carolina, March 2-5, 1986, p. 492, American Nuclear Society (1986).

26. M. EDENIUS, K. SMITH and D. M. VER PLANCK, "New Data and Methods for CASMO and SIMULATE," *Proc. Topl. Mtg. Reactor Physics*, Saratoga Springs, New York, September 17-19, 1986, Vol. 2, p. 1115, U.S. Nuclear Regulatory Commission (1986).

27. P. JERNBERG, "CASMO-3 Benchmarks Against Criticals," STUDSVIK/NFA-86/11, Studsvik (1986).

28. P. RASHID, "CASMO-3 Benchmark Against Yankee Rowe Isotopics," STUDSVIK/SOA-86/5, Studsvik (1986).

29. "Improvements in EPRI-CELL and Benchmarking of the ENDF/B-V Cross Section Library," NP-2416, Electric Power Research Institute (1982).